

Lessons learned from VISIR

E. Pantin^a and C. Doucet^a and H.U. Käuff^b and P.O. Lagage^a and R. Siebenmorgen^b and M. Sterzik^c

^aDSM/DAPNIA/SAP, CE Saclay, UMR 7158, FRANCE;

^bESO Garching, GERMANY;

^cESO Chile, Chile;

ABSTRACT

VISIR is the VLT mid-infrared (mid-IR) Imager and Spectrometer. Since 2004, it provides data at high spatial and spectral resolutions in the N (8-13 μm) and Q (16-24 μm) atmospheric windows. VISIR observations have provided unique constraints on targets such as central regions of nearby galaxies, or protoplanetary disks. We review here VISIR Imager and Spectrometer characteristics, emphasizing on some current limitations because of various undesirable effects. Its successor on an ELT will provide data with a unique sharpness (0.05") and sensitivity (35 μJy source detectable in 1 hour at 10 σ level), thus allowing a characterization of exoplanetary disks and inner exoplanets with an unprecedented precision. At the light of VISIR experience, we discuss how the lessons learned from VISIR can be turned to good account for designing and operating the future mid-IR instrument on the European ELT.

Keywords: Mid-infrared, VISIR

1. VISIR INSTRUMENT

VISIR is mounted on the VLT unit Melipal at Paranal and has been commissioned in April 2004. Since April 2004, it operates routinely to deliver mid-infrared (mid-IR) images and spectra in N (R=300 to 30000) and Q (R=1500,15000) atmospheric bands¹, (see Fig.1). The data are diffraction limited in the N band if the optical seeing is below ~ 0.8 arcsec (see Sec.4.1); Q band imager data are almost always diffraction limited. The high

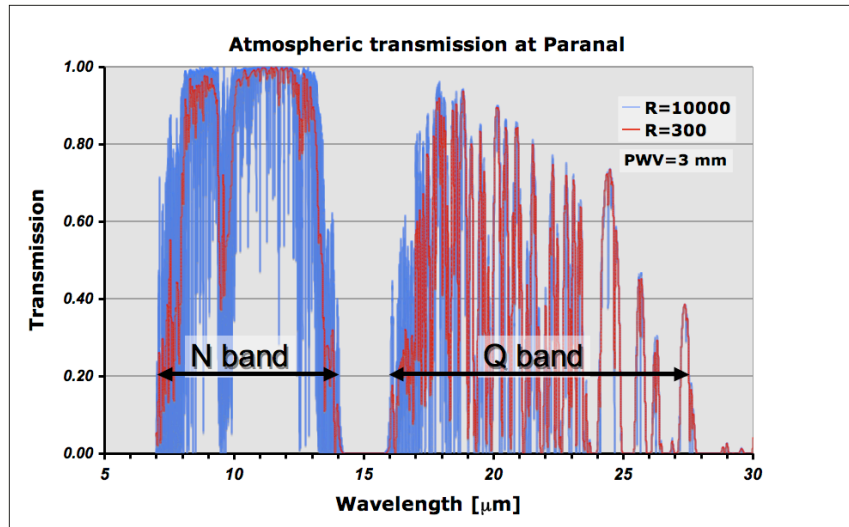


Figure 1. Mid-IR atmospheric transmission at Paranal site for medium weather conditions. The transmissions at two spectral resolutions are displayed.

Further author information: (Send correspondence to E.P.)

E-mail: eric.pantin@cea.fr, Telephone: 33 1 69 08 71 31

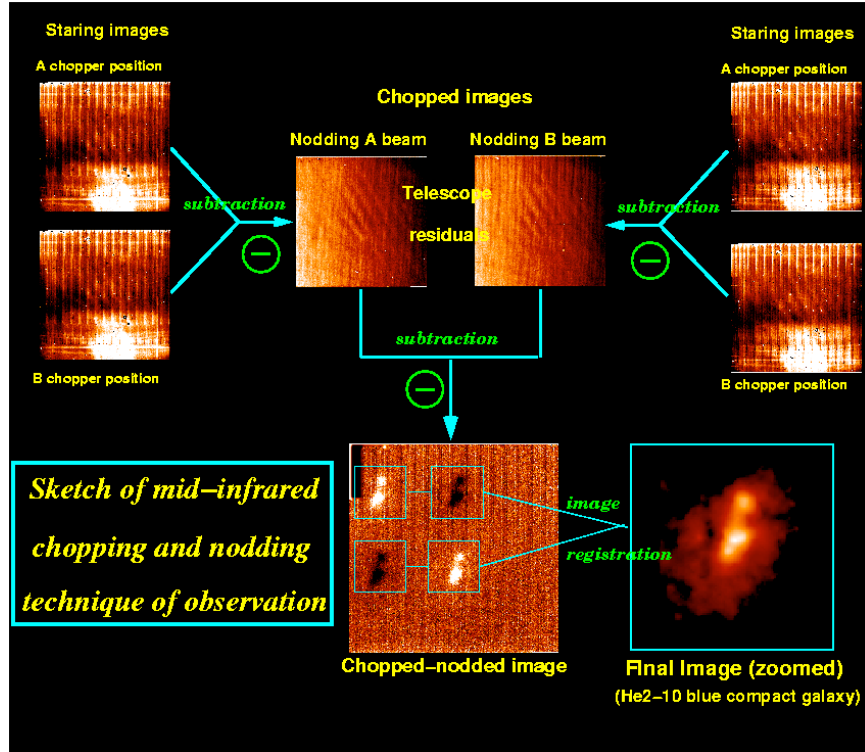


Figure 2. Scheme of chopping and nodding technique used to suppress the high mid-IR background. First, the elementary (staring frames) images are averaged over half a chopping period. Then, the chopping correction is applied for each telescope nodding position. Finally, chopping residuals due to different optical paths in the 2 chopper positions, are canceled by subtracting the two nodding beams. If the field on the detector is large enough, the four beams can be maintained in the field of view and, apart from beam switching overheads, no telescope time is loss.

spectral resolution mode is unique in the southern hemisphere; it offers for instance the possibility to perform observations of the warm H_2 pure vibrational modes at 8.02, 9.66, 12.28, 17.03 μm or the NeII line at 12.81 μm . Given the overwhelming background emitted by both the atmosphere and telescope, background canceling techniques are compulsory (Fig.2). The instrument itself emits a negligible background since its interior is cryogenically cooled between 50 and 70 K. VISIR Imager uses typical chopping frequencies around 0.25 Hz and nodding period around 1 minute.

1.1 Detectors

VISIR contains two DRS detectors, one in the imager, one in the spectrometer. They have well-capacities around $2.10^7 e^-$ (large capacity mode) and $2.10^6 e^-$ (small capacity mode). Quantum efficiency is typically around 50%. A detailed study of the detectors characteristics can be found in Ref.2. The detectors working point is nominally set around +5000 ADU on the sky (1 ADU \approx 275 e^- , given a total range of [-32000,32000] ADU). The detectors start to saturate at levels higher than 8000 ADU and more (about 2/3 of the total capacity). Some pixels have an abnormal behavior (gain) and will trigger striping (detector striping, due to multiplexer amplifiers collapse, see Fig.3) over a usually wide range of rows on the detector. This striping is periodic, with a period of 16 pixels, since one amplifier reads every 16 pixels sequentially. A strong source on the detector will also produce (although at a higher level) the same type of effect, the source striping, on any pixel. A first order correction of source striping can be achieved by estimating the stripes pattern in a 256x16 sub-frame free of any source, and subtracting this pattern to all other (15) 256x16 sub-frames. See Ref.3 for a more complete description of all possible (including more evolved) methods. Given the level of the background, the detector dark current (smaller than 7000 e^-) and readout noises (1771 and 296 e^- in high and low capacity modes) are negligible against the background shot noise. Rapid imaging experiments have been performed in order to study any other source of noise. These

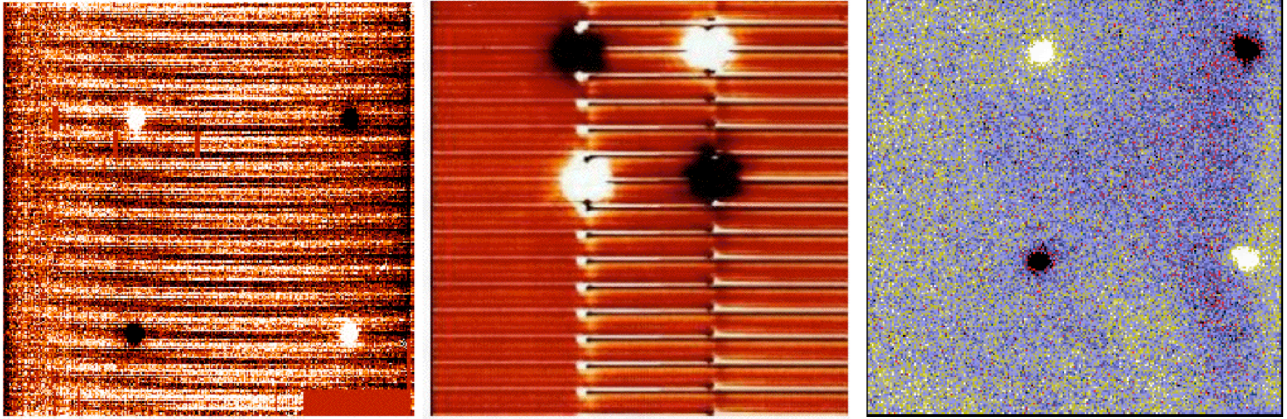


Figure 3. Left and middle panels : Imager data showing the “striping effect”. On the left side, the “detector striping” at low level on top of a faint point source is shown. This striping is periodic (16 pixels) and depends at first order, on background fluctuations that affect “hot” pixels. On the middle panel is shown the ”source striping”, triggered by the a strong source. Right panel shows the background residuals underneath a relatively faint source (Comet Tempel 1). The background excess excess of noise at low spatial frequencies appears as “valleys and hills” (see Sec.3)

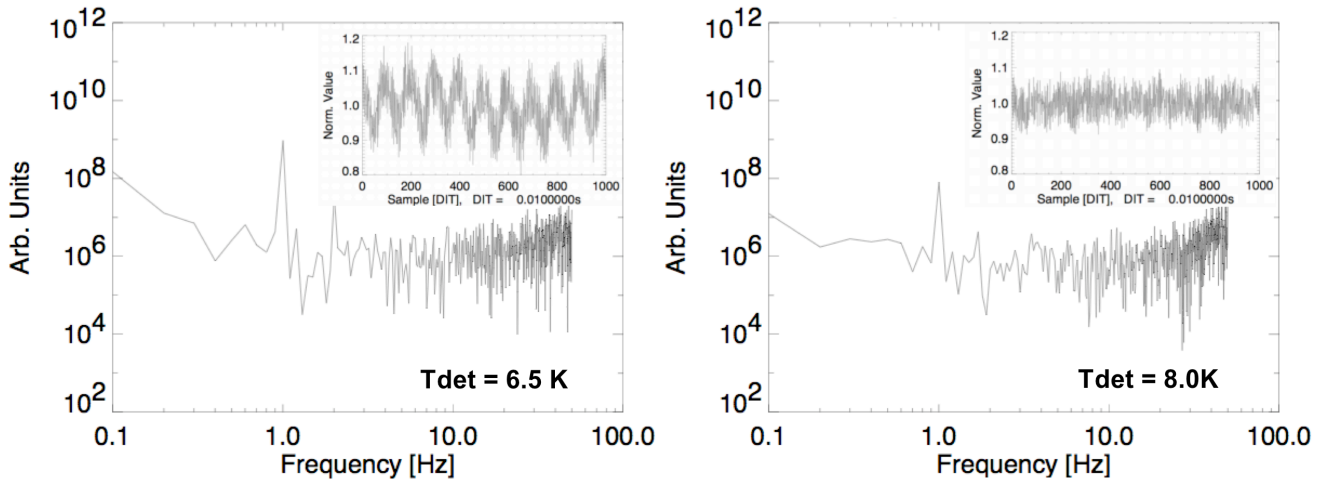


Figure 4. Detector output power spectrum as a function of the detector temperature (inset are the time signals). At 6.5K, a clear 1Hz fluctuations noise is evidenced. At 8.0K, the 1 Hz noise is significantly reduced. In both cases, no other obvious periodic noise is evidenced; above few Hertz, the noise is almost white as expected.

experiments show that a too low temperature of the detector (6.5 K), a 1 Hz periodic noise generated by the cryocoolers pulse tube is appears (see Fig.4). When slightly increasing the working temperature of the detector to 8.0K, these thermal oscillations vanish (see Fig.4), but at the expense of the detectors cosmetics (increase of detector striping). At 8.0 K also, the shot noise increases as expected (square-root of impinging number of photons), whereas its behavior seems more erratic and less easily interpretable at 6.5 K. A detectors upgrade for the Raytheon 1kx1k Aquarius detectors is planned in a near future.

1.2 Warm Calibration Unit (WCU)

On top of VISIR enclosure lies the Warm Calibration Unit (WCU). This unit comprises a point source (monochromator), and extended source (Peltier plate) presenting an adjustable surface temperature ($[-20,50]^{\circ}\text{C}$) and a

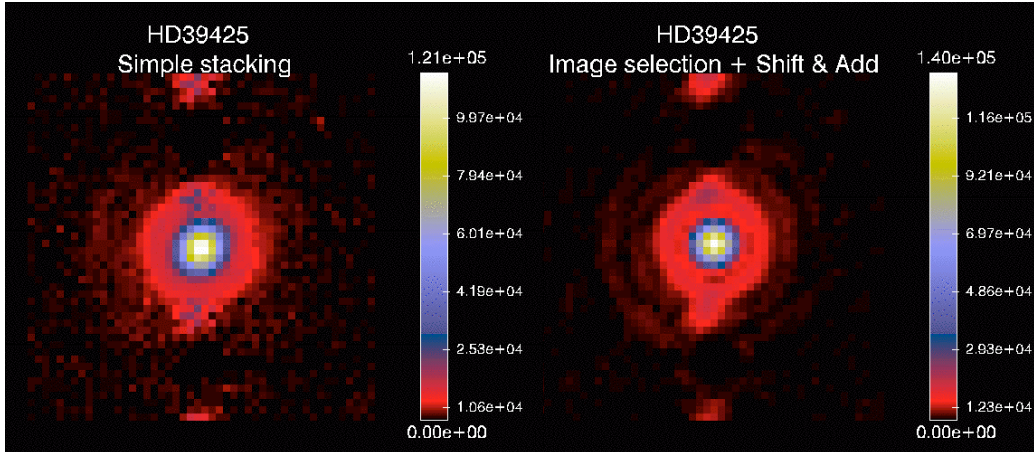


Figure 5. Left panel : simple stack of burst mode frames of the standard star HD39425, simulating a classical observation. Right panel, shift-and-add and image selection are applied to burst mode data. The average FWHM is decreased by 15% and the Strehl ratio is improved from 0.52 to 0.65. Note also the two unveiled diffraction rings (dark red) appearing in right panel.

telescope simulator (Offner design). This unit allows to perform daytime checks and calibrations (e.g. image quality, relative sensitivity, flat-field measurements, filter transmission curves).

1.3 “Burst Mode”

The burst mode is a fast readout mode in which all the elementary (DIT) frames are recorded. Obtained at frame rates in the range 10-100 Hz ($T=10-100$ ms), they offer various possibilities over standard data : speckle imaging (complementary to MIDI4), shift-and-add to correct for turbulence tip-tilt or any external PSF deformation/tilt and recover diffraction-limited data⁵, see Fig.5. However, 1) the source has to be clearly detectable (e.g. a source flux larger than 1 Jy in PAH2 filter) to properly shift-and-add (after eventual frames selection) the frames. 2) Since the chopper is not synchronized with the instrument operating system, the data reduction is rather complex; in particular, the chopper phase has to be estimated. 3) The instrument efficiency is quite affected in this mode; the ratio total time/time shutter open increases from ~ 1.5 to ~ 2.5 .

2. OBSERVING AND CALIBRATING MID-INFRARED DATA

Relevant quality control parameters are the precipitable water vapor content (PWV), the background level, and the sensitivity. The data themselves contain valuable informations to calibrate the data (e.g. sky lines for wavelength calibration). Weather observational parameters are relatively stable over few hours, thus only a limited number of standard star interlaced observations are really needed for photometric calibration purpose.

2.1 Sensitivity

VISIR imager measured sensitivities over the period Sep. 04-May 08 are reported in Fig.6. The median sensitivities ($\sim 4-5$ mJy/ 10σ /1h in the best N-band filter, ~ 50 mJy/ 10σ /1h in Q-band) are close, within a factor of 2, to expected theoretical values. The point source sensitivities in N band are remarkably stable in time and under various weather conditions; Q band ones are much more sensitive to the precipitable water vapor content and airmass. The same conclusions apply to the spectrometer data. See Ref.6 for a detailed analysis of spectrometer sensitivities.

2.2 Photometry

Imager conversion factors (which allows to convert from ADU to physical units (e.g. Jy)) are frequently monitored on a selection of standard stars from Cohen’s radiometric catalogue. The value depends mainly on the external conditions (pwv, dust content and temperature of the atmosphere, telescope temperatures), but shows very small

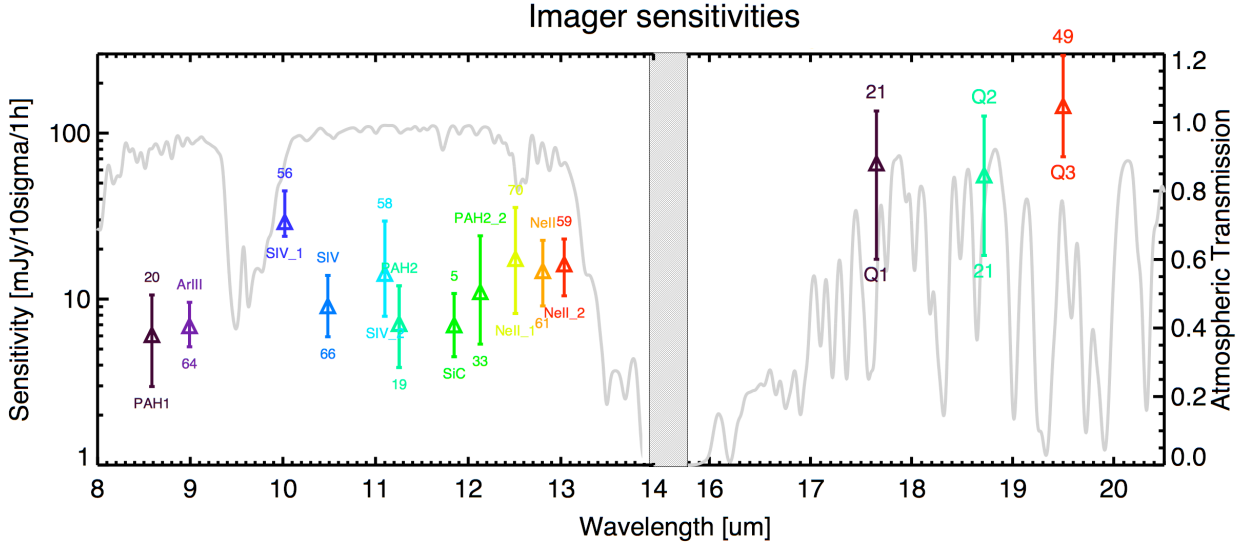


Figure 6. Sensitivities of the VISIR Imager, for all filters, in N and Q bands, for the smallest field of view (75 mas/pixel). The triangles mark the median sensitivities over the period 2004-2008; the vertical bars are bounded by the values of the first and fourth quartiles of measured sensitivities. The spectral resolutions for each of the filters are also given. In gray is overlotted a low-resolution atmospheric transmission model for Paranal (3mm PWV).

variations ($\leq 10\%$ in N band) from one night to another. This means that a decent photometry at a 10% precision level can be obtained on a “standard conditions” night by using simply the median value of monitored conversion factors over one year. Recent observations of asteroids (bright point sources) using VISIR show that a careful photometric analysis of data taken under fairly good conditions lead to typical $\sim 3\%$ and $\sim 4.5\%$ photometric error levels in N and Q bands respectively⁷. However, the final photometric precision on faint, slightly extended sources becomes extremely limited not any longer by the background shot noise, but by the background residuals shown in Sec.3.

Spectrophotometric calibration is also achieved on the same standard stars, but in the specific case of high-resolution spectra data, the use of bright asteroids leads to a better telluric calibration.

2.3 PSF calibration

Thanks to the relatively low impact of the seeing on the angular resolution of N-band data, the spatial accuracy, mainly diffraction-limited as long as the optical seeing is lower than 0.8 arcsec (FWHM $\sim 0.25-0.3$ arcsec), should be in principle easily calibratable using interlaced observations of standard PSF stars. Q-band imager data are almost always diffraction-limited (FWHM $\sim 0.5-0.6$ arcsec). However in practice, even if the optical seeing has often a median value close or lower the above limit, its possible rapid variations render the PSF calibration difficult. On top of that, the uncertainty on the PSF calibration is strengthened by a variable in time (and unpredictable) ellipticity. The same effect seems altering also the FWHM measurements as a function of wavelength in spectrometer low-resolution mode, because the N-band is sliced into four settings (thus potentially 4 different PSFs). See Fig.7 for further details. VISIR image deconvolution is consequently very challenging. With such conditions, standard PSF deconvolution methods (such as Richardson-Lucy, and any wavelets based by-products⁸) become unapplicable. One alternative to recover a diffraction-limited PSF is to use the Burst Mode followed by a careful data reduction in which the PSF-degraded frames are discarded and the retained frames are stacked using a good shift-and-add algorithm (see Fig.5).

2.4 Spectrometer specificities

VISIR data contain both sky-subtracted images and sky data. Sky spectra can be usefully compared to models of mid-IR atmospheric emission to derive in most of the cases an accurate enough wavelength calibration. In the

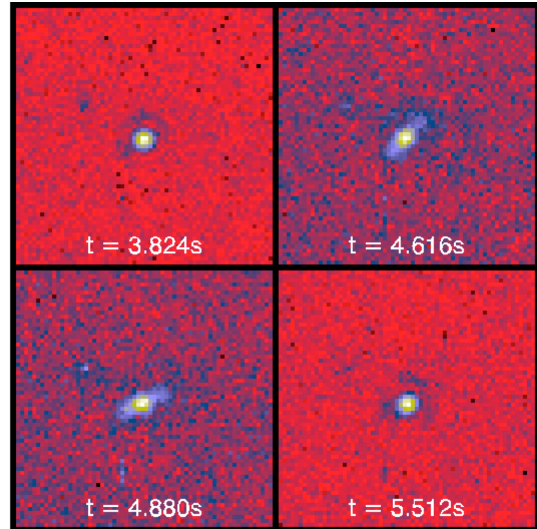
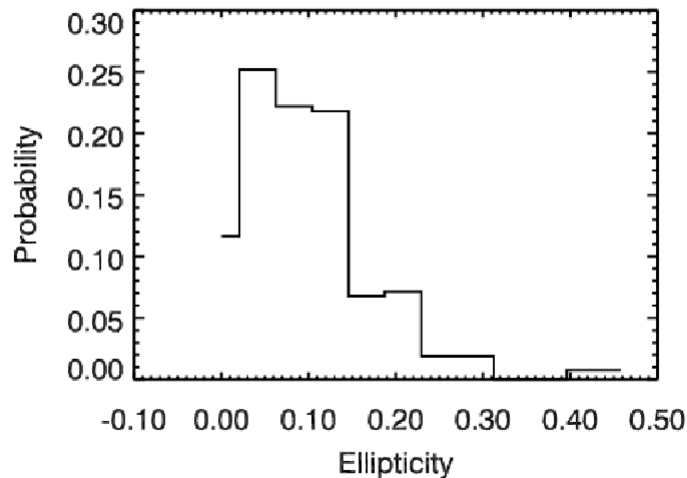


Figure 7. Left panel : histogram of observed PSF standard stars ellipticities. According to this analysis, about 20% of VISIR observations shall have distorted PSFs with ellipticities larger than 0.15 (the ellipticity is defined as $1 - \text{fwhm}_{\min}/\text{fwhm}_{\max}$); in other words, an ellipticity of 0.15 reflects a difference of 0.15% in FWHM between the horizontal and the vertical axis). Typical PSF distortions on a 2s timescale are evidenced in real time when examining burst mode data in which the data are recorded at a frame rate of 125 Hz.

majority of the cases, except some very “clean” windows in N-band at medium and high resolution, it is possible therefore to “self-calibrate” the data.

N-band low-resolution spectra ($R \sim 300$) often suffer from significant photometric absolute errors. A full N-band spectrum can be only obtained through a sequence of 4 low-resolution settings, stitching errors between the different settings are often observed (Fig.8). An correct absolute spectrophotometry of the individual settings can be however obtained if some narrow-band imaging data have been taken in each of the spectrometer settings. A similar problem is evidenced with full-width at half maximum measurements of an target as a function of the wavelength.

2.5 Flat-fieldability

Photometric standard stars observations show typical photometric variations of a few percent on the 4 different beams in the most sensitive N-band filter (PAH2), the dispersion has a standard deviation of about 1%. The background shot-noise contributes to about typically 0.5% in the photometric error and therefore, cannot explain a few percents of variation peak-to-peak. The observed variations must be then attributed either to background errors (see 3), or to a spatially varying differential response of the detector. Background errors (Sec.3) cannot account for the full photometric variations observed; on the other hand laboratory measurements of the detectors gains show peak-to-peak variations of about 1% on individual pixels gains.² To reach the highest photometric accuracy, it would be probably interesting to correct for individual pixels responses, however, estimating them is not an easy task. On one hand, sky dips are affected by instrument flexures, on the other hand, observations of the extended source of the warm calibration unit and varying its plate temperature can be corrupted by temperatures variations on the light path. So far, flat-fielding attempts did not improve the photometric accuracy.

3. BACKGROUND CANCELLATION AND ERRORS

The background errors appear as residual, non flat, slowly varying structures in VISIR images (Fig.3, rightmost panel). On the other hand, background noise measurements on the sky show a departure from the expected noise levels as soon as the chopping frequency is lower than ~ 1 Hz (Fig.9, left panel). A spatial scale analysis finally shows that the noise excess is mainly located a mid- and low-spatial frequencies (Fig.9, right panel). A natural interpretation is that a too low chopping frequency (0.25 Hz) produces the observed residual background

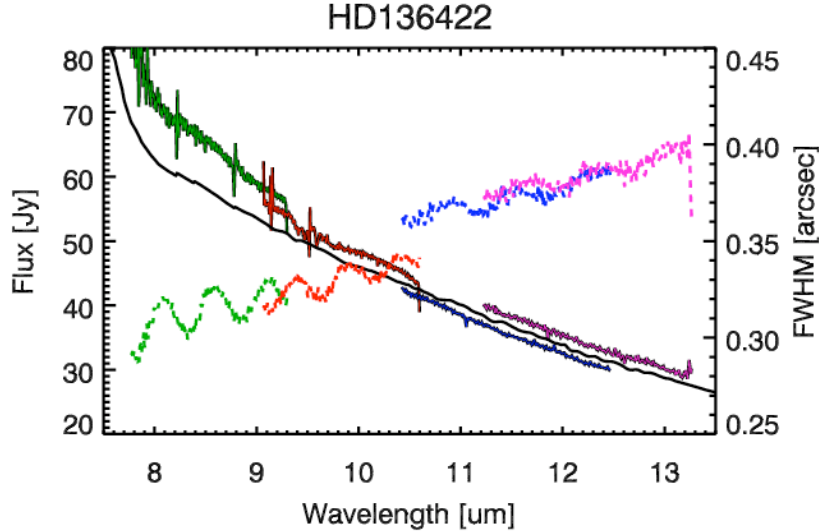


Figure 8. Low-resolution spectra of a standard star (HD136422) in the four settings covering the N band. The observation has been corrected for telluric absorption using a second calibration star. The VISIR observed spectra are discontinuous between two adjacent settings, which evidences of a photometric miscalibration. The black line represents the true HD136422 spectrum. The dashed lines display the FWHM measurements of HD136422 low-resolution spectra.

structures in VISIR images. This background error limits severely the achievable photometric accuracy on faint, extended sources (the more extended, the higher the uncertainty). A first order correction can be “manually” made by hiding the source in VISIR images and reconstructing underlying background using 2D spline or bilinear interpolation on the nearest source neighbors pixels. However, this method is highly biased by the *a-priori* definition of the source support. Alternative methods, based on multiresolution inpainting scheme, provide much better results.³

Future mid-infrared instruments should benefit from large format (1kx1k) and flat-fieldable detectors better stability of the gains). In an ideal case, detectors with a gain known at a $10^{-(4-5)}$ level of accuracy would significantly decrease the constraints concerning the background cancellation techniques, especially on an ELT.

4. HIGH LEVEL PROCESSING

4.1 Image deconvolution

VISIR on a 8.2m telescope reaches the limits of purely diffraction-limited instruments. Assuming an atmospheric turbulence following a Kolmogorov distribution of turbulence cells (seeing $\lambda^{-1/5}$), the seeing value around 10 μm is roughly half of that in the visible range. VISIR mid-infrared data should thus not be longer diffraction limited as soon as the optical seeing becomes larger than 0.7 arcsec. Burst VISIR data allows to carefully analyze the tip-tilt fluctuations of standard star images, and then derive macroscopic turbulence parameters such as the Fried parameter R_0 . Our measurements give $R_0 = 6.23 \pm 0.33$ m at 8.6 μm and $R_0 = 8.76 \pm 0.42$ m at 11.3 μm when the optical is 0.75 arcsec. They confirm that VISIR data become seeing-limited at 10 μm for an optical seeing larger than ~ 0.75 arcsec. In these conditions, mid-infrared image deconvolution becomes a much more difficult problem to solve. Standard methods which assume an almost perfectly calibrated PSF, such as Landweber, Richardson-Lucy, or more modern wavelets based ones will produce wrong solutions. Myopic deconvolution methods are a must in this case but require a large, redundant, dataset.⁸

5. MAIN RESULTS BY ASTRONOMY DOMAIN

Several key questions in astronomy are best tackled by observations in the Mid-IR. In the following we present two recent achievements which are based on VISIR data, a first one is concerned with properties of galactic nuclei and a second one with the structure of proto-planetary disks.

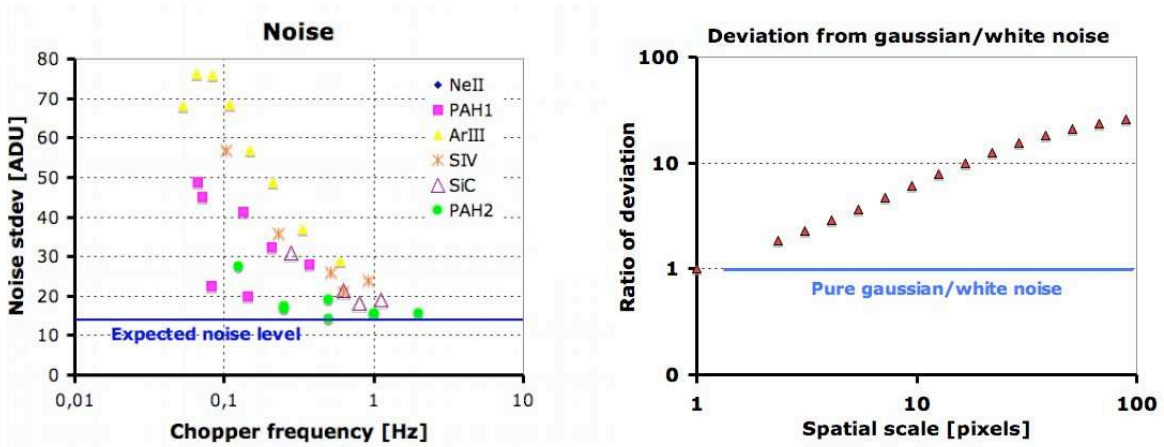


Figure 9. Left panel : measurements of the background noise as a function of the chopping frequency, for various N-band filters of VISIR. Depending on the filter, an increase of noise for chopping frequencies smaller than ~ 1 Hz is evidenced. Note also the correlation between the noise excess and the presence of atmospheric lines in the filter (e.g. ArIII filter ($9 \mu\text{m}$) spans a large number of atmospheric lines, while PAH2 one ($11.25 \mu\text{m}$) depends much less on the chopping frequency). Right panel : analysis of the excess noise in PAH1 filter ($8.6 \mu\text{m}$) as a function of the spatial frequency. At a spatial scale of 10 pixels, the noise is about 10 times larger than expected if the noise had a white spatial distribution.

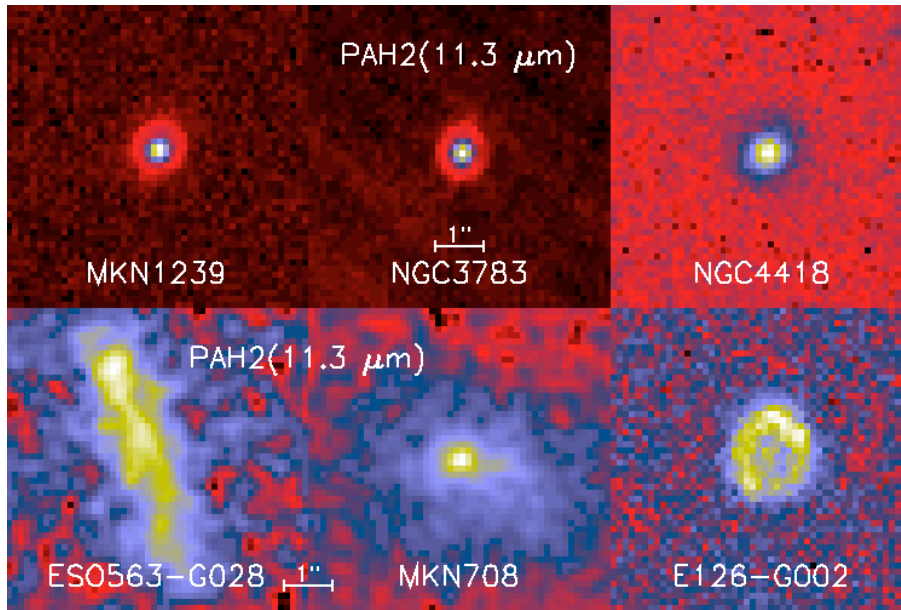


Figure 10. Nuclear MIR emission of nearby galaxies as revealed by VISIR (spatial resolution: $0.35''$ (FWHM), $11.3 \mu\text{m}$ filter). While AGNs (top) remain unresolved at high surface brightness, starbursts (bottom) show extended emission of up to a few arcsec at much lower surface brightness⁹.

5.1 Extragalactic infrared astronomy

The Mid-IR luminosity of the central region of galaxies has long been known to be a reliable indicator of activity and is much less affected by dust extinction than optical and NIR observations. The Mid-IR emission traces thermal radiation from hot dust ($\sim 100\text{K}$) heated either by OB stars or black hole activity. Many diagnostics have been proposed to quantify which of the two activity types, starburst (SB) or active galaxies nuclei (AGN), is dominant. At the spatial resolution of VISIR it is found that AGN and SB can now be clearly separated using the nuclear Mid-IR surface brightness, S , as criterion: AGNs appear to be dominated by an unresolved core at

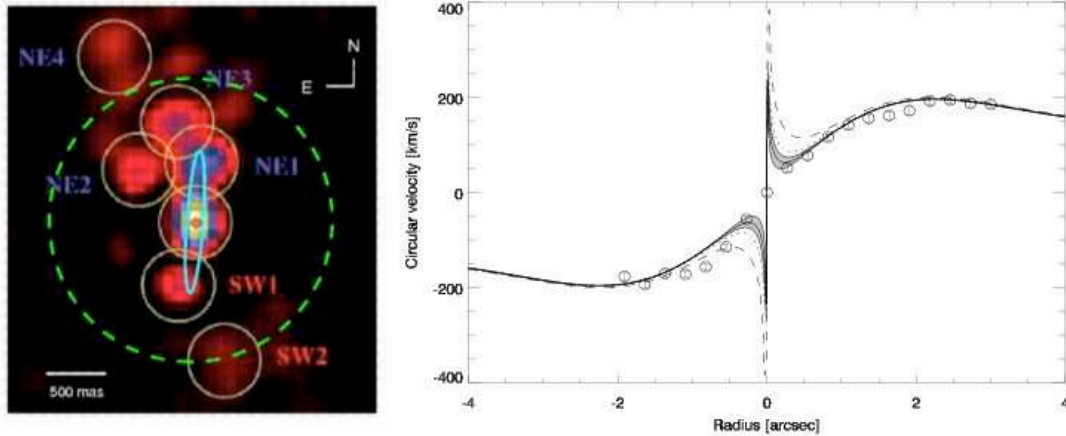


Figure 11. Left panel : NGC1068 as observed with VISIR (underlying image) and MIDI (red dot, green and blue contours). MIDI detects an intermediate scale ($2''$) mid-IR emission (green dashed contour); VISIR resolves it into several knots. Right panel : velocity resolved VISIR data of the active galaxy NGC7582 using the high-resolution spectrograph of VISIR at $12.8 \mu\text{m}$ (NeII line). The velocity curve of inner obscured regions allows to determine an upper limit on the mass of the central black hole.

$S \geq 10,000 L_{\odot}/\text{pc}^2$ whereas SB show extended structure of the nucleus of several arcsec at $S \sim 1000 L_{\odot}/\text{pc}^2$ (see Fig.10). A few examples are shown in Fig.11. This technique to separate AGN - SB activity requires the resolving power of an 8m class telescope and is still limited to distances of up to 100 Mpc or at an ELT to ≤ 500 Mpc, respectively. It cannot be applied to data obtained from the ground by a 4m class telescope or using space-born telescopes.

A key question in modern astronomy is the formation of galaxy and related to this is the process of black hole formation and growth. To advance knowledge good observational techniques are required to estimate the black hole mass. One method is to apply the tight correlation between black hole mass and stellar velocity dispersion as derived from optical data. Unfortunately such direct measurements of black hole mass are challenging because of the high spatial resolution required and the high dust enshrouding of the nucleus. Both limitations could be overcome by recent VISIR MIR high resolution ($R \sim 16000$) spectroscopy of the [NeII] $12.8 \mu\text{m}$ line. The VISIR data provided for the first time a black hole mass estimate in an external galaxy by MIR observations and from the rotational potential of the stellar bulge a central black hole mass of $\leq 5.5 \times 10^7 M_{\odot}$ was found in NGC7582 (see Fig. 11 right panel, and Ref.10).

5.2 Low-mass companions and protoplanetary disks

ϵ Indi B is the closest brown dwarf binary system known. The sources separation is only $0.73''$. SPITZER observatory is thus unable to study individually each of the components. VISIR observations, although penalized by a much lower sensitivity, resolved them and put constraints on the physical characteristics of both components (see Ref.11).

HD97048 is a young (3 Myr) intermediate-mass Herbig star of the Chameleon cloud, surrounded by a protoplanetary disk of dust and gas. VISIR direct imaging in PAH bands (8.6 and $11.3 \mu\text{m}$) have resolved for the first time the structure of the disk (Ref.12 and Fig.12). The disk is thick, dense, and has a flaring upper surface as predicted by Kenyon & Hartmann¹³. The measured flaring index (1.26 ± 0.05) is strikingly close to the expected value of $9/7 = 1.28$ obtained when assuming hydrostatic equilibrium of the disk. VISIR high spectral resolution observations confirmed the presence of warm gas (0.01 to 1 Jupiter masses) by detecting the H_2 emission line at $17.035 \mu\text{m}$ (see Fig.12). Maybe more important, the gas to dust mass ratio measured in the inner 35 AU (3000 to 14000) significantly departs from the canonical value of 100 (Martin-Zaïdi et al.¹⁴); maybe due to planet formation inducing dust depletion.

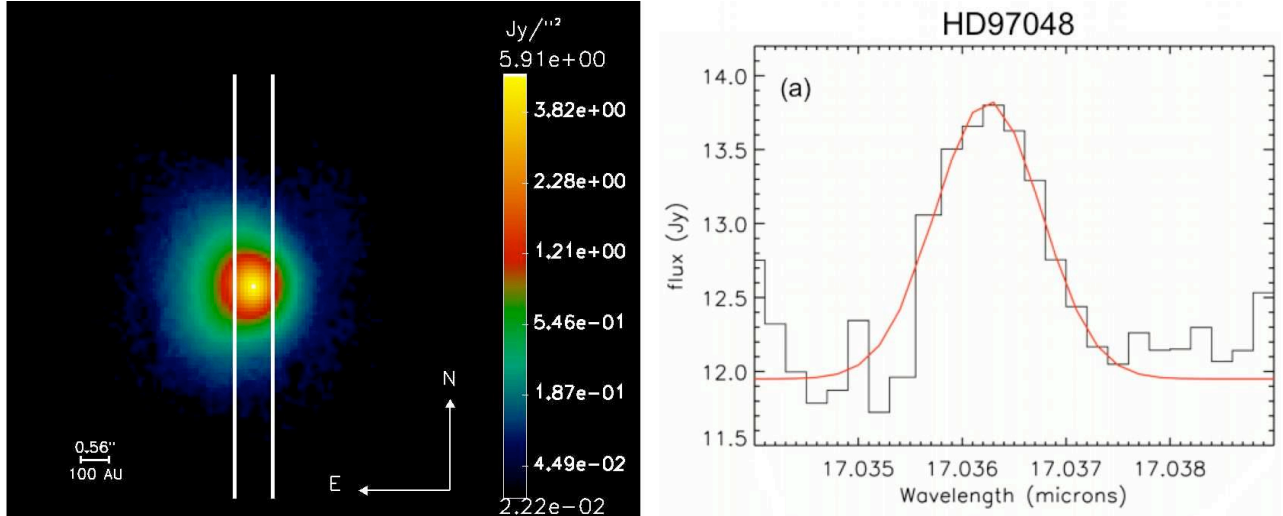


Figure 12. Left panel : the HD97048 dust disk resolved in VISIR image at $8.6 \mu\text{m}$. For the first time, a precise measure of the flaring index β ($H \propto r^\beta$, where H is the scale height of the disk at a distance r from the star) of a proto-planetary disc around an intermediate-mass star has been achieved. Right panel : the 0-0 S(1) H_2 emission line detected in HD97048 (0.75 arcsec wide slit overplotted on left panel).

6. OBSERVING IN THE MID-INFRARED RANGE ON AN ELT

The expected sensitivities in the mid-IR on an ELT open some new perspectives in the field of exoplanetary sciences. Low-resolution spectroscopy of giant planets on orbits of a few AUs from the parent star would allow to better characterize their atmospheric composition and mass. Inner ($r \leq 0.4$ AU) "super-Earth" massive telluric exoplanets radii would be marginally directly detected around the closest stars ($d \leq 3\text{pc}$). Finally, a ELT mid-IR instrument, given its sensitivity and spatial resolution is a perfect tool to accurately study protoplanetary and debris disks. In particular, structures such as gaps would be quite easily revealed.

The awaited performances of a mid-IR instrument depend critically on the observatory site. N-band observations are [1.2-1.3] times more sensitive at a high altitude site (4500 m) than at Paranal. This factor reaches even a value of 5 for Q-band observations (see Fig.13). In addition, the Q-band extends further at higher wavelength as the precipitable water vapor (PWV) content in the atmosphere (highly reduced at higher altitudes) decreases. In particular, quite clean intermediate band windows ($R \sim 30$) open at 24.5 and $27.3 \mu\text{m}$ (see Fig.13). In combination with the angular resolution provided by an extremely large telescope, we get a unique instrument able to study circumstellar/circumnuclear materials at intermediate temperatures ($T=100\text{K}$), bridging the gap between the well studied characteristics of the targets around $10 \mu\text{m}$ and far-infrared/sub-millimetric observations.

In order to be competitive with space-born infrared observatories, high spatial and spectral resolutions shall be the drivers to build ground-based mid-IR instruments. The ELT theoretical diffraction limit can be maintained in the mid-IR range at a moderate cost, i.e. using relatively simple adaptive optics system when compared to near-IR ones. Most of the science cases described in this paper deal with targets angularly very close to a stronger source (star, central engine of an AGN); this implies very tight constraints on the temporal stability of the components (telescope, AO front-end, instrument). Moreover, the peak value of a typical 1 Jy source observed with an ELT will be three times larger the background level; spurious detector saturation effects will probably arise. Stability and accuracy can be recovered by using coronagraphic devices in combination with simultaneous differential imaging.

7. CONCLUSIONS AND PERSPECTIVES

Important science cases, requiring either high spatial or spectral resolution, can be uniquely addressed by ground-based mid-IR astronomy. Although mid-IR data are generally very demanding in terms of data reduction efforts,

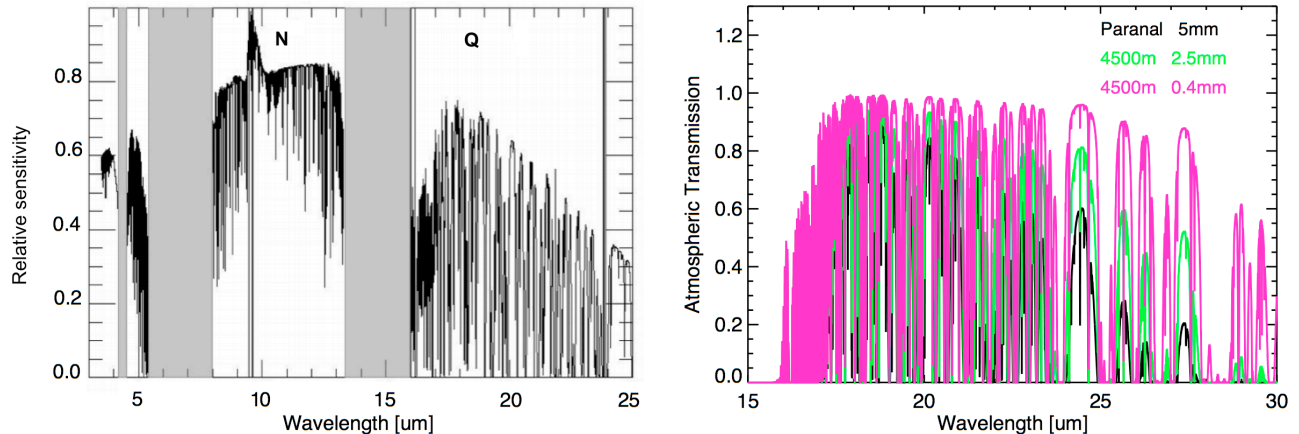


Figure 13. Left panel : ratio of ground-based mid-IR point-source sensitivity between Paranal and a site at an altitude of 4500 m. right panel : atmospheric transmissions in Q band as a function of the site/altitude. Paranal site (altitude = 2450 m) with a PWV of 5 mm (poor conditions) is taken as the reference. A higher altitude site (4500 m) is considered, in 2 cases : poor PWV conditions (2.5 mm) and good ones (0.5 mm). Note the large gains in transmissions at highest wavelength.

the results can lead to unique scientific break-through, sometimes unachievable at any other wavelength. VISIR on the VLT offers to the astronomers a very large palette of observing modes, some of which are unique in the Southern hemisphere. VISIR potentialities are still affected by restrictive factors such as detector striping or PSF stability. However, hardware (detectors upgrades) or operational (burst mode) solutions are foreseen to obtain the best scientific return from VISIR.

A mid-IR ELT instrument will have unique combination of spatial resolution and point source sensitivity (0.05 arcsec/35 μ Jy in 1h), but such an instrument would largely increase in sharpness (especially concerning differential measurements) if devices such as four quadrants coronagraphs, or dual-band imaging would be implemented. In such conditions, not only such an instrument would be "the perfect machine" to study dusty disks, but direct characterization of exoplanetary systems would be achievable.

ACKNOWLEDGMENTS

The authors thanks the scientific and technical staff of Paranal for their valuable help and their strong involvement in setting VISIR into operations. The author thanks T. Müller for allowing to report his results on asteroids observations with VISIR.

REFERENCES

- [1] Lagage, P. O., Pel, J. W., Authier, M., Belorgey, J., Claret, A., Doucet, C., Dubreuil, D., Durand, G., Elswijk, E., Girardot, P., Käufel, H. U., Kroes, G., Lortholary, M., Lussignol, Y., Marchesi, M., Pantin, E., Peletier, R., Pirard, J.-F., Pragt, J., Rio, Y., Schoenmaker, T., Siebenmorgen, R., Silber, A., Smette, A., Sterzik, M., and Veyssiere, C., "Successful Commissioning of VISIR: The Mid-Infrared VLT Instrument," *The Messenger* **117**, 12–16 (Sept. 2004).
- [2] Galdemard, P., Garnier, F., Mulet, P., and Reynolds, D., "Characterization of DRS Technologies' 256x256 mid-IR arrays for VISIR," in [*Instrument Design and Performance for Optical/Infrared Ground-based Telescopes. Edited by Iye, Masanori; Moorwood, Alan F. M. Proceedings of the SPIE, Volume 4841, pp. 129-140 (2003).*], Iye, M. and Moorwood, A. F. M., eds., *Presented at the Society of Photo-Optical Instrumentation Engineers (SPIE) Conference* **4841**, 129–140 (Mar. 2003).
- [3] Pantin, E., "VISIR data processing and enhancement," In preparation (Sept. 2008).

- [4] Poncelet, A., Doucet, C., Perrin, G., Sol, H., and Lagage, P. O., “An original interferometric study of NGC 1068 with VISIR BURST mode images,” *A&A* **472**, 823–831 (Sept. 2007).
- [5] Doucet, C., Lagage, P., and Pantin, E., “High resolution Mid-Infrared Imaging of Dust Disks Structures around Herbig Ae Stars with VISIR,” in [*Visions for Infrared Astronomy, Instrumentation, Mesure, Métrologie*], Coudé Du Foresto, V., Rouan, D., and Rousset, G., eds., 25–30 (2006).
- [6] Smette, A. and L.Vanzi, [*VISIR Users Manual*], ESO, ESO (2008).
- [7] Müller, T., Pantin, E., Kaasalainen, M., Durech, J., Hormuth, F., and Sterzik, M., “Thermophysical characterisation of 16 main-belt asteroids with VISIR,” In preparation (Sept. 2008).
- [8] Pantin, E. and Starck, J.L. Murtagh, F., “Deconvolution and blind deconvolution in Astronomy,” in [*Blind Image deconvolution : Theory and Applications*], Campisi, P. and Egiazarian, K., eds., 100–138, CRC Press (May 2007).
- [9] Siebenmorgen, R., Haas, M., Pantin, E., Krügel, E., Leipski, C., Käuffl, H., Lagage, P., Moorwood, A., Smette, A., and Sterzik, M., “Nuclear activity in nearby galaxies,” Submitted (May 2008).
- [10] Wold, M., Lacy, M., Käuffl, H. U., and Siebenmorgen, R., “The nuclear regions of NGC 7582 from [Ne II] spectroscopy at 12.8 μm - an estimate of the black hole mass,” *A&A* **460**, 449–457 (Dec. 2006).
- [11] Sterzik, M. F., Pantin, E., Hartung, M., Huelamo, N., Käuffl, H. U., Kaufer, A., Melo, C., Nürnberger, D., Siebenmorgen, R., and Smette, A., “The cool atmospheres of the binary brown dwarf ϵ Indi B,” *A&A* **436**, L39–L42 (June 2005).
- [12] Lagage, P.-O., Doucet, C., Pantin, E., Habart, E., Duchêne, G., Ménard, F., Pinte, C., Charnoz, S., and Pel, J.-W., “Anatomy of a Flaring Proto-Planetary Disk Around a Young Intermediate-Mass Star,” *Science* **314**, 621–623 (Oct. 2006).
- [13] Kenyon, S. J. and Hartmann, L., “Spectral energy distributions of T Tauri stars - Disk flaring and limits on accretion,” *ApJ* **323**, 714–733 (Dec. 1987).
- [14] Martin-Zaïdi, C., Lagage, P.-O., Pantin, E., and Habart, E., “Detection of Warm Molecular Hydrogen in the Circumstellar Disk around the Herbig Ae Star HD 97048,” *ApJ* **666**, L117–L120 (Sept. 2007).